Deuteron Compton Effect*†

R. S. JONES, H. J. GERBER,‡ A. O. HANSON, AND A. WATTENBERG
Department of Physics, University of Illinois, Urbana, Illinois
(Received June 18, 1962)

Elastic scattering by deuterons of photons between 190 and 250 MeV has been measured by exposing a liquid deuterium target to the bremsstrahlung beam of the University of Illinois 300-MeV betatron. The scattered photons were detected by a lead glass total absorption-type Čerenkov counter, and the recoil deuterons were momentum analyzed in a magnetic field and detected by a scintillation counter telescope. The observed cross sections in the center-of-momentum system, in Thomson proton units of $(e^2/M_p)^2=2.35\times10^{-32}$ cm²/sr, are, for a photon c.m. scattering angle of 140°, 0.879±0.10 at 189 MeV and 0.751±0.11 at 219 MeV; and for a photon c.m. scattering angle of 110°, 0.943±0.13 at 218 MeV and 1.47±0.26 at 250 MeV. These values are compared with those using the neutron and proton amplitudes predicted by dispersion relations and employing the impulse approximation, and with the exception of the point at 189 MeV are found to be consistent with the theoretical calculations.

INTRODUCTION

THE present experiment is a measurement of the cross section for the elastic scattering of photons by deuterons above the photopion production threshold. By means of such a measurement, it is possible to study the neutron-photon scattering amplitude. Experimental work on both the proton and deuteron Compton effect has already been carried out.[1,2] Furthermore, there are several theoretical calculations for these phenomena.[3–6] Additional references, as well as a complete discussion of the corresponding proton scattering experiment, are given by Bernardini *et al.*[1] Several more recent papers cover measurements and calculations of the proton Compton effect in the region of 300 MeV and above.[7–10] The present work has previously been published in preliminary form.[11,12]

Most of the theories for the proton Compton effect correctly reproduce the essential features of the data: a marked rise in the cross section at energies above 200 MeV and a peaking of the differential cross section for backward angles. Several of the recent theories calculate the cross section by using available data from photopion production to evaluate dispersion integrals. This approach was first suggested by Gell-Mann, Goldberger, and Thirring,[4] and refinements of it have been made by Capps[5] and by Jacob and Mathews.[6]

A measurement of the deuteron Compton effect has been made by Hyman *et al.* in the region below the pion threshold.[2] A theoretical calculation for this cross section was carried out by Capps.[5] In the present paper we have applied the Jacob and Mathews[6] amplitudes to the deuteron problem by following Capps' recipe. The formulas for the deuteron cross section provided by these two theories, as well as curves for them calculated on the University of Illinois ILLIAC, are given in the Appendix.

The information on the neutron must be inferred from a deuteron measurement and this has been our approach. Thus we shall be checking the validity of combining the neutron and proton amplitudes in the bound deuteron system, by means of the impulse approximation.

METHOD OF THE EXPERIMENT

In this experiment we have attempted to obtain some data in order to find out whether the deuteron cross section has the expected energy dependence. Four points were measured in the energy range of 190–250 MeV, all above the photopion production threshold.

There are two principal experimental difficulties: (1) distinguishing the Compton events from those caused by neutral pion production in deuterium, and (2) separating elastic and inelastic deuteron events.

The two competing processes which must be distinguished are

$$\text{(a)}\ \gamma+d\rightarrow d'+\gamma'$$
$$\text{(b)}\ \gamma+d\rightarrow d'+\pi^0\rightarrow d'+\gamma'+\gamma''$$

The energy of the Compton scattered photon is not very different from that of one of the π^0 decay photons, for a given initial energy incoming γ ray in the energy range of 150–250 MeV. However, the different recoil

* This research was supported in part by the U. S. Office of Naval Research.
† Based on a thesis (R. S. Jones) submitted in partial fulfillment of the requirements for the degree of Doctor of Philosophy.
‡ Present address: CERN, Geneva, Switzerland.
[1] G. Bernardini, A. O. Hanson, A. C. Odian, T. Yamagata, L. B. Auerbach, and I. Filosofo, Nuovo cimento **18**, 1203 (1960) and T. Yamagata, Ph.D. thesis, University of Illinois, 1956 (unpublished).
[2] L. G. Hyman, R. Ely, D. H. Frisch, and M. A. Wahlig, Phys. Rev. Letters **3**, 93 (1959). In a private communication from D. Luckey, recent measurements are reported as follows: ratios of deuterium to hydrogen differential cross section for Compton scattering of photons between 70 MeV and 120 MeV are 1.32±0.09 at 90° and 1.30±0.10 at 135°, with an absolute laboratory cross section for hydrogen at 90° of (1.18±0.18)×10⁻³²cm².
[3] B. T. Feld, Ann. Phys. (New York) **4**, 189 (1958).
[4] M. Gell-Mann, M. L. Goldberger, and W. E. Thirring, Phys. Rev. **95**, 1612 (1954).
[5] R. H. Capps, Phys Rev. **106**, 1031 (1957); **108**, 1032 (1957)
[6] M. Jacob and J. Mathews, Phys. Rev. **117**, 854 (1960).
[7] K. Berkelman, Nuovo cimento **21**, 633 (1961).
[8] A. P. Contogouris, Nuovo cimento **21**, 674 (1961); Phys. Rev. **124**, 912 (1961).
[9] J. W. DeWire, M. Feldman, V. L. Highland, and R. Littauer, Phys. Rev. **124**, 909 (1961).
[10] L. G. Hyman, Phys. Rev. **125**, 1765 (1962).
[11] R. S. Jones, Ph.D. thesis, University of Illinois, 1961 (unpublished).
[12] R. S. Jones, H. J. Gerber, A. O. Hanson, and A. Wattenberg, Bull. Am. Phys. Soc. **6**, 430 (1961).

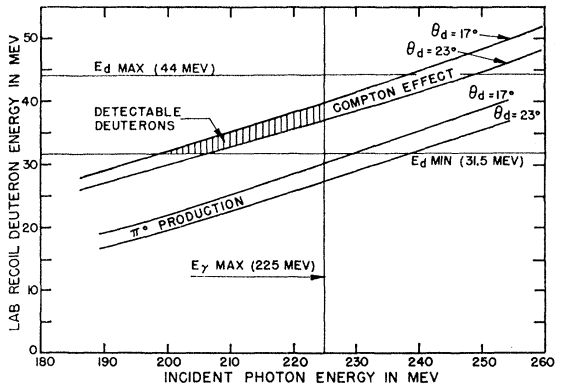

FIG. 1. Dynamical separation of the Compton scattering and neutral pion production processes in deuterium.

deuteron energies can be well separated by an analyzing magnet, so that by properly choosing the maximum bremsstrahlung energy and the magnet momentum selection interval of recoil deuterons in coincidence with photons, all the neutral pion background can be eliminated. This is illustrated in Fig. 1, in which, as a function of incident energy photons, the momentum of the recoil deuterons is plotted at constant recoil angles for both the π^0 and Compton processes.

The second problem, that of separating the inelastic from the desired elastic events was accomplished by displaying the pulses from the three counters on an oscilloscope, photographing the traces, and analyzing them with regard to pulse height and time of flight. The information obtained proved more than adequate for distinguishing protons and deuterons, and a reliable deuteron count could be made.

Experimental Setup

A schematic diagram of the experimental setup illustrating the essential equipment is shown in Fig. 2. The basic equipment consists of a liquid deuterium target located in the betatron bremsstrahlung beam and in which the Compton scattering of γ rays occurs, the lead glass Čerenkov counter which detects the scattered γ rays, the deflecting magnet which, together with its entrance and momentum apertures, selects the recoil deuterons in a given momentum range, and the deuteron

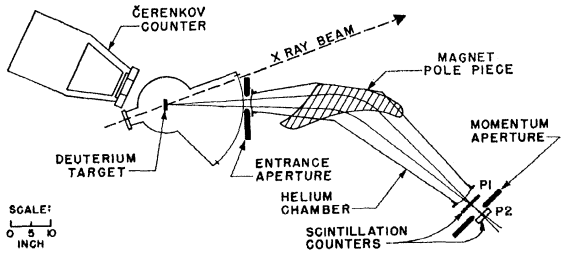

FIG. 2. Plan view of experimental arrangement.

detection telescope consisting of two plastic scintillation counters.

The x-ray beam from the betatron passes through a "clearing field" which sweeps out secondary electrons and enters the vacuum system of the liquid deuterium target.[1] The x rays traverse the deuterium which is contained in a lens-shaped vessel called the appendix, situated at the "optical" source point of the magnet. The appendix has an average thickness of 1.5 cm over the 1-in.-diam circular cross section of the beam. This choice of thickness is a compromise between the desire for a high counting rate and the need to eliminate energy loss of recoil deuterons in the target itself which affects the measured energy resolution of the incoming γ rays.

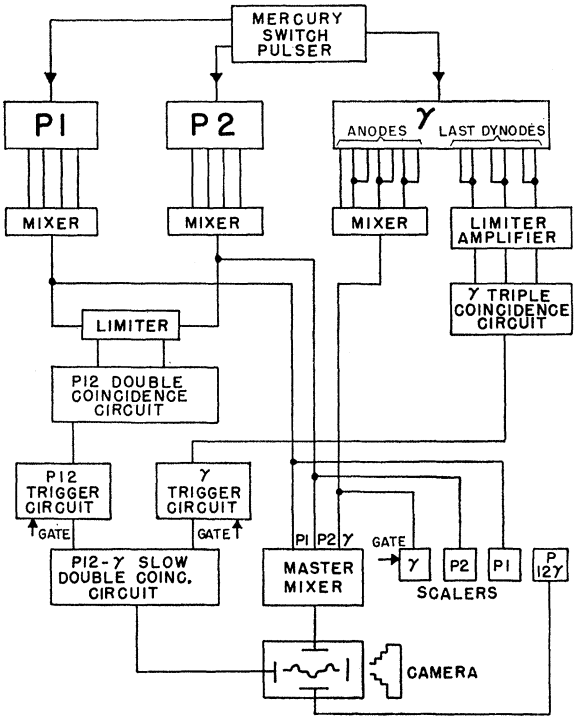

FIG. 3. Block diagram of electronics.

The scattered photons are detected by the Čerenkov counter, which has for an entrance collimator, a 2-in.-thick lead ring with an 11-in. o.d. and a $4\frac{1}{2}$-in.-diam hole at its center. This aperture subtends a cone at the target of half-angle approximately 12.5° and is chosen so as to intercept all photons from Compton events for which recoil deuterons enter the defining aperture of the magnet. The Čerenkov counter itself is a nondirectional lead glass total absorption type, whose pulses have a height proportional to the total energy of the incoming γ rays. This counter, together with its associated electronics, is described in detail in the preliminary report of this work.[11]

The recoiling deuterons enter a helium-filled magnetic analyzer through a rectangular aperture cut in a 1-in.-

thick brass plate. This aperture, which determines the solid angle, subtends at the target a horizontal angle of $\pm 2°$ and vertical one of $\pm 1.8°$, and is effectively outside the magnetic field.

The width of the lead slit system, at the "optical" image point of the magnet, together with the magnet current setting, determine the momentum or energy interval for the deuterons which are detected by the counter telescope.

This detection system consists of two counters, each about 6 in. wide and 9 in. high. The first, $P1$, is a $\frac{1}{16}$-in.-thick plastic scintillator transmission counter whose pulse height is approximately proportional to dE/dx, and the second, $P2$, is a $1\frac{1}{4}$-in.-thick plastic scintillator stopping counter whose pulse height is a measure of the total energy, E.

Electronics

The electronic system, whose block diagram is shown in Fig. 3, is separated into two major chains: (1) the display chain, whose purpose is to collect and to amplify the pulses, and to deposit them on the 100-nsec/cm sweep of the Tektronix 517 oscilloscope, and (2) the trigger chain, whose purpose is to start the sweep for any event having some characteristics of a Compton scattering.

Experimental Procedure

Prior to the main run, several preliminary checks were made. The first consisted of a relative calibration of the analyzing magnet and the betatron. This was accomplished by comparing a "floating wire" calibration of the magnet with that of the betatron by observing the maximum energy positrons produced by the betatron bremsstrahlung beam. An uncertainty of $\frac{1}{2}\%$ in this intercalibration is the chief source of experimental error which ranges between $\pm 5\%$ and $\pm 15\%$ in the cross-section measurements.

An experimental check was made to verify that deuterons recoiling from π^0 production were not observed when the system was set to detect Compton deuterons. For a given betatron energy and recoil deuteron direction, it is possible to choose the magnet momentum in such a way that all π^0 deuterons do not have sufficient energy to pass through both the entrance and the exit apertures of the magnet, while Compton deuterons have. To check this point experimentally, it was only necessary to move the Čerenkov counter away from the correct angle set for a Compton run. No events were observed during a time sufficient to collect approximately 25 events.

Further checks included short π^0 photoproduction runs for both hydrogen and deuterium.

The main runs consisted of four measurements of the cross section of the deuteron Compton effect. First with the magnet at 20°, the betatron was run at 225 and at 200 MeV. Then with the magnet rotated to 35°, the betatron settings were 255 and 225 MeV.

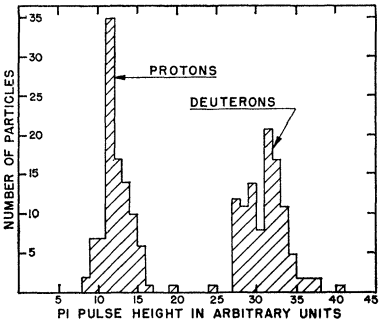

FIG. 4. Pulse-height distribution for the $P1$ counter for $\theta_d = 35°$, $E_\gamma^{\max} = 225$ MeV, and central magnet selection momentum = 297 MeV/c.

It was necessary in all of these runs to set the magnet current and apertures so that only the top part of the bremsstrahlung spectrum was used in order to prevent the detection of recoil deuterons in π^0 production. This resulted in very low counting rates, of the order of one or two deuterons per hour. Some accidentals were present at full betatron intensity but were always distinguishable from true deuteron or proton events after inspection of the film.

During the runs the magnet current was monitored with a potentiometer to prevent drifts, and the Hall voltage of the Halltron field monitor was periodically read as a second check on the absolute magnetic field settings.

Counting rates for each of the counters, $P1$, $P2$, and γ, as well as for the $P12\gamma$ triple coincidences, were frequently observed as a check on the stability of the apparatus. Another check was made on the entire electronic system every hour by means of a mercury switch pulser.

Data Analysis

Three pulses, $P1$, $P2$, and γ, were displayed on the scope trace and photographed. These pulses were arbitrarily spread out over 600 nsec, with $P1$ and $P2$ at the ends of this time interval and γ approximately at its center.

Typical pulse-height distributions for the $P1$ and $P2$ pulses are illustrated in Figs. 4 and 5. The deuterons and protons appear well resolved. This separation is shown strikingly in Fig. 6, where a sort of three-dimensional histogram is plotted in two dimensions, i.e., the number of counts vs $P1$ and $P2$ pulse heights. Pulses of almost zero height are visible on the film, which indicates that

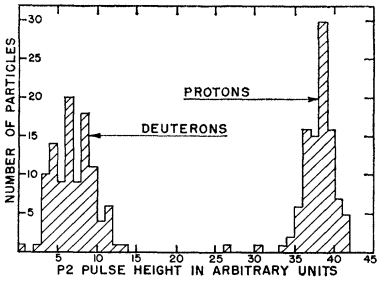

FIG. 5. Pulse-height distribution for the $P2$ counter for $\theta_d = 35°$, $E_\gamma^{\max} = 225$ MeV, and central magnet selection momentum = 297 MeV/c.

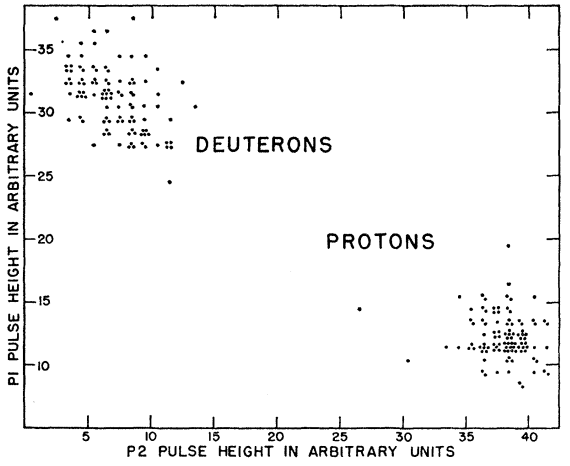

FIG. 6. Pulse-height correlation between the $P1$ and $P2$ counters for $\theta_d=35°$, $E_\gamma^{\max}=225$ MeV, and central magnet selection momentum=297 MeV/c.

the trigger levels were set low enough so that the scope would certainly fire on all true events.

The second independent method for distinguishing among deuterons, protons, and background was the measurement of the time difference between the $P2$ and γ pulses. A plot of the number of pulses against this time difference is shown in Fig. 7. The interval of about 33 nsec between the protons and deuterons in part (a) of the figure agrees quite well with the calculated value.

EXPERIMENTAL RESULTS

Deuteron Compton Effect Cross Section

The relation of the various experimentally measured quantities to the laboratory differential scattering cross section $(d\sigma/d\Omega)^{\text{lab}}$ is as follows:

$$(d\sigma/d\Omega)^{\text{lab}}=D/N_d\Delta\Omega N_\gamma, \quad (1)$$

where D is the observed number of Compton recoil deuterons per erg of x-ray energy through the target, N_d is the number of deuterium atoms in the target per cm^2 averaged over the beam area, $\Delta\Omega$ is the laboratory deuteron solid angle, and N_γ is the effective number of photons striking the target per erg of x-ray energy through the target. A typical effective photon spectrum from which N_γ is calculated is shown in Fig. 8. It is seen to be the product of the bremsstrahlung spectrum $n(E_\gamma)$ and the experimental counting efficiency function $F(E_\gamma)$ which is determined by the angle and momentum intervals accepted by the magnetic analyzer. The bremsstrahlung spectrum used in the evaluation of the cross section is taken from a formula of Schiff as tabulated by Leiss.[13]

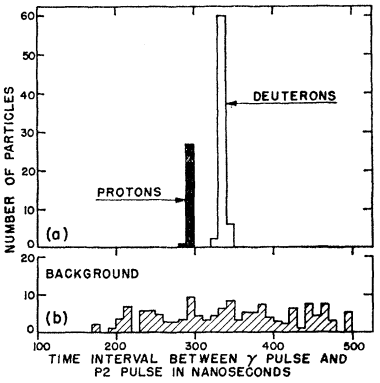

FIG. 7. Time analysis of pulses for $\theta_d=20°$, $E_\gamma^{\max}=200$ MeV, and central magnet selection momentum=297 MeV/c.

The experimentally measured cross sections are given in Table I together with the pertinent experimental quantities. The differential cross section is given in two forms: (1) in the laboratory system in terms of the deuteron solid angle, in units of cm^2/sr, and (2) in the center-of-momentum (c.m.) system in terms of the photon (or deuteron) solid angle, in Thomson proton units $(e^2/M)^2=2.35\times10^{-32}$cm^2/sr. Also plotted in these figures are the corresponding theoretical curves based on the work of Capps[5] and of Jacob and Mathews.[6] The horizontal flags on the points in Fig. 9 represent the half-widths of the effective photon spectra, which are indicated along the horizontal axis.

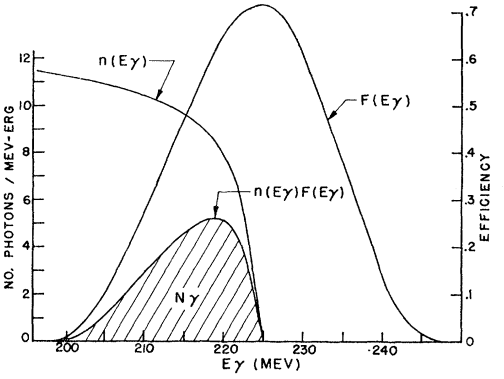

FIG. 8. Effective photon number and spectrum in the efficiency calculation for $\theta_d=20°$, $\theta_\gamma=136°$ and $E_\gamma^{\max}=225$ MeV. The quantities in the figure are related by the formula: $N_\gamma=\int_0^{E\gamma\max} n(E_\gamma)F(E_\gamma)dE_\gamma$, where $n(E_\gamma)$ is the Schiff bremsstrahlung spectrum and $F(E_\gamma)$ is the experimental efficiency for counting Compton deuterons recoiling from a gamma ray of energy E_γ.

The errors listed with the tabulated measurements and shown on the graphs are compounded from counting statistics and from the uncertainty in the effective photon flux.

Neutral Pion Production Cross Section

The π^0 photoproduction cross section for deuterium was measured at 238 MeV. The value together with pertinent experimental data is listed in Table I. The measured cross section is about 15% higher than a corresponding value interpolated from the calculation of

[13] J. E. Leiss (private communication).

TABLE I. Results.

Experimental conditions	Deuteron Compton Effect				Neutral Pion Production
Betatron energy (MeV)	200	225	225	225	250
Magnet angle (lab)	20°	20°	35°	35°	20°
Magnet aperture (lab)	±2°	±2°	±2°	±2°	±2°
Magnet current (Am)	131.4	248.0	131.4	248.0	187.5
Momentum aperture[a] (cm)	±2.5	±2.5	±2.5	±2.5	±2.5
Deuteron recoil energy at center of magnet (MeV)	23.3	32.3	23.3	32.3	28.0
Experimental results					
Energy of effective photon number spectrum peak (MeV)	189	219	218	250	238
Range of half-max width of eff photon number spectrum (MeV)	179–198	209–224	208–223	242–254	229–248
Photon angle (lab)	132°–141°	132°–140°	99°–108°	98°–108°	123°–132°[b]
Sticking factor $S(q)$	0.123	0.089	0.128	0.083	
$(d\sigma/d\Omega_d)^{\text{lab}}$ (10^{-32}cm^2/sr)	7.83±0.9	6.67±0.9	7.28±0.1	11.3±2.3	768±61
$(d\sigma/d\Omega)^{\text{c.m.}}/(e^2/M)^2$	0.879±0.10	0.751±0.11	0.943±0.13	1.47±0.26	131±10[c]

[a] 0.55 cm = 1% deuteron momentum spread.
[b] π^0 angle.
[c] $(d\sigma/d\Omega_\gamma)^{\text{lab}}$.

Ramakrishnan, Devanathan, and Ranachandran[14] which compares favorably with earlier experimental work.

THEORY AND COMPARISON WITH THE RESULTS

The theoretical analysis of the deuteron Compton effect has been carried out by Capps[5] as an extension of his work on the proton. His approach is to estimate the neutron amplitudes and then to combine them with the proton amplitudes in some suitable way.

The neutron amplitudes are obtained from those of the proton simply by modifying the static components of the proton amplitudes so that they correspond to the charge and magnetic moment properties of the neutron, while the mesonic parts are left unchanged. This calculation neglects nucleon recoil leading to possible errors of the order of 15%. In the case of the neutron there is, of course, no Thomson term and therefore the spin-independent amplitudes are not depressed at forward angles. The spin-dependent amplitudes are the same as the proton exhibiting a rise in the backward angles. Thus the neutron exhibits a forward and a backward rise as a result of the sum of the spin-dependent and spin-independent parts, whereas the proton in which the spin-independent amplitudes destructively interfere with the Thomson amplitude at forward angles exhibits only a backward peaking.

The problem of combining the neutron and proton amplitudes is handled by means of the impulse approximation. The fundamental assumption of the impulse approximation is that amplitudes from the two nucleons can simply be added linearly to obtain the amplitude for the whole system. The conditions for this assumption are discussed by Chew and Lewis,[15] who point out that the large deuteron radius (about 4.3 F) makes it a favorable system for the application of the impulse approximation. Capps estimates inaccuracies in the impulse approximation to be not larger than 0.3 e^2/M.

The impulse approximation expression for the deu-

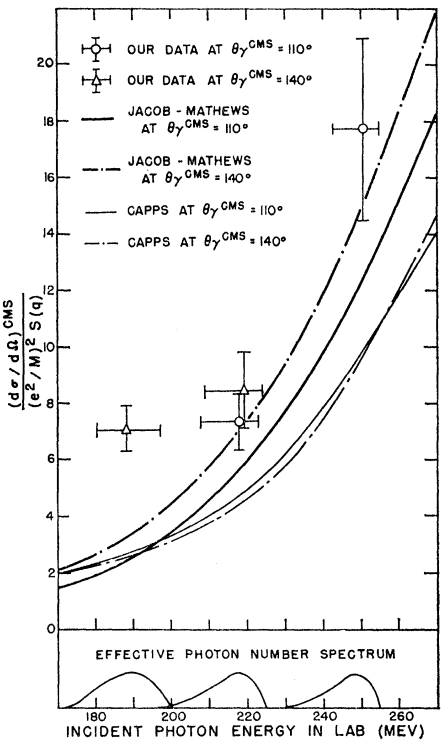

FIG. 9. Measured and calculated differential cross sections for the deuteron Compton effect in the center-of-momentum system, divided by the sticking factor, $S(q)$, and in terms of the Thomson proton unit $(e^2/M)^2$. Along the horizontal axis are indicated the effective photon spectra used in the evaluation of the measured cross sections.

[14] A. Ramakrishnan, V. Devanathan, and G. Ranachandran, Nuclear Phys. 24, 163 (1961).
[15] G. F. Chew and H. W. Lewis, Phys. Rev. 84, 779 (1951).

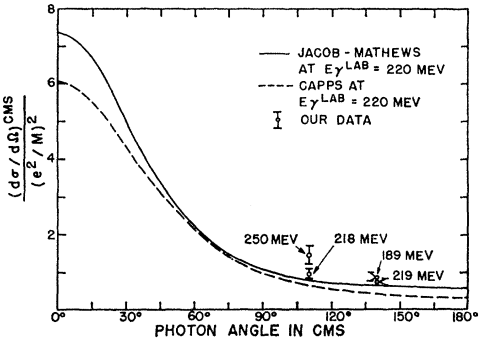

FIG. 10. Experimental points and calculated differential cross sections in the center-of-momentum system (CMS) as a function of the c.m. scattered photon angle.

teron cross section as derived by Capps is

$$d\sigma/d\Omega=[|A_p+A_n|^2+\tfrac{2}{3}|B_p+B_n|^2]S(q), \qquad (2)$$

where $d\sigma/d\Omega$=elastic differential scattering cross section of photons from deuterons, $A_{p,n}$=spin-independent amplitude for proton or neutron, $B_{p,n}$=spin-dependent amplitude for proton or neutron, and S(q) is the so-called "sticking factor," defined as the square of the momentum transform of the deuteron wave function:

$$S(q)=F^2(q),$$
$$F(q)=\int d^3r\, e^{-iq\cdot r}\phi^2(r), \qquad (3)$$

where $\phi(r)$ is the radial part of the deuteron wave function.

The square bracket in (2) represents the basic photon-nucleon interaction, and the interference between the spin-dependent parts of the neutron and proton amplitudes and between the spin-independent parts is shown explicitly. The second term represented by $S(q)$ gives the probability that the two nucleons will stick together after the collision.

In calculating $S(q)$, Chew used a Hulthén wave function for the deuteron. However, since the sticking factor is formally the square of the form factor, we have taken the values from the analysis of the electron-deuteron scattering data of McIntyre and Burleson,[16] which are compatible with deuteron wave functions derived from a hard core potential. The values of the sticking factor, used in the interpretation of this experiment, are listed in Table I.

We have made two theoretical estimates of the elastic scattering of photons from deuterium. The first employs Capps' formula, which we have arbitrarily extrapolated to 250 MeV in order to compare it with our data. (Capps, however, gives for the region of validity of his expressions, 100 to 200 MeV.) The second calculation was performed using the Jacob and Mathews amplitudes for scattering from protons, by first constructing the neutron amplitudes by means of charge independence, and then combining the neutron and proton amplitudes according to the impulse approximation recipe. The complete Capps and Jacob and Mathews expressions and a set of calculated curves are given in the Appendix.

The calculated curves are shown in Fig. 9 and 10 along with the experimental data. In Fig. 9, where the energy dependence of the center of momentum system cross section is shown, the "sticking factor" has been divided out in order to compare more directly with the proton Compton effect. The experimental cross section as a function of energy had much the same shape as that of the proton data: exhibiting the sharp resonance rise above 200 MeV. Our deuteron measurements, however, lie higher than the theoretical curves. At 250 MeV the Jacob-Mathews value is about 25% (1.5 standard deviations) lower than the measured cross section. At 220 MeV the theoretical values are, respectively, 10% (6.7 standard deviations) and 21% (1.5 standard deviations) lower than the measured 110° and 140° values. The theoretical cross section at 190 MeV is lower than the experimental one by about 50% (5 standard deviations).

The angular dependence of the differential cross section is shown in Fig. 10. There are only two points at the same energy (220 MeV) and two different angles (θ_γ=110°, 140°) so that a thorough comparison with theory is not possible. The expected drop, however, in going from 110° to 140° is clearly exhibited. (In the calculations, the sticking factor actually reverses the rising angular dependence of both the neutron and proton amplitudes.)

In view of the strong dependence of the calculations of the deuteron Compton effect on the sticking factor, and the small number of experimentally measured points, it is generally difficult to make a detailed comparison between theory and experiment. Although the sticking factor values used agree well with the existing experimental data,[16] they are small enough (of the order of 0.1) so that small variations in the sticking factor produce relatively large effects in the calculated cross section. Accordingly, not too much significance is placed on the difference between the calculations and the measured cross sections for the three higher energy points. Even the apparent better agreement of the Jacob and Mathews theory with these three points is not unexpected in consideration of the fact that the Capps theory has been "pushed" beyond its region of validity. Thus within the experimental and theoretical inaccuracies, the three higher energy measurements are consistent with the calculation of the neutron amplitudes

[16] J. A. McIntyre and G. R. Burleson, Phys. Rev. **112**, 2077 (1958).

from those of the proton by means of charge independence.

However, the point at 190 MeV seems to be in disagreement with the theories. There is no experimental reason at present to doubt this 190-MeV value, although it is a single point with no support from other evidence. Currently, however, a new measurement is in progress at Illinois and if this discrepancy persists, it could prove to be quite interesting theoretically, inasmuch as 190 MeV is in the energy region of strong interference among the several contributing amplitudes.

ACKNOWLEDGMENTS

The authors are very much indebted to the staff of the betatron and especially to L. Rogers, J. Harlan, and G. Schwab. We should also like to thank Professor J. D. Jackson, Professor D. G. Ravenhall, and Professor R. L. Schult for helpful discussions and suggestions regarding the calculations. Dr. A. C. Odian was very instrumental in initiating this effort. Mrs. D. C. Lee has been most helpful in designing and building the liquid deuterium target system. It is a great pleasure to acknowledge the many contributions of R. Abrams and of R. Parsons to the experiment. We are also indebted to J. Ehrman for calculating the theoretical curves with the use of the University of Illinois ILLIAC.

APPENDIX. THEORETICAL FORMULAS AND CURVES FOR DEUTERON COMPTON EFFECT

Capps Theory[5]

$$(d\sigma/d\Omega)^{\text{c.m.}}=(e^2/M)^2(k_d/k_l)^2S(q)$$
$$\times\{\tfrac{1}{2}(1+\cos^2\theta)(|A^E|^2+|A^M|^2)$$
$$+\cos\theta[|A^E+A^M|^2-|A^E|^2-|A^M|^2]$$
$$+\tfrac{1}{3}(3-\cos^2\theta)(|B^E|^2+|B^M|^2)$$
$$+\tfrac{2}{3}\cos\theta[|B^E+B^M|^2-|B^E|^2-|B^M|^2]\},$$

$$A^E=A_p{}^E+A_{n'}{}^E \quad A_n{}^E=A_p{}^E+1,$$
$$A^M=A_p{}^M+A_{n'}{}^M \quad A_n{}^M=A_p{}^M+k_l/2M,$$
$$B^E=B_p{}^E+B_{n'}{}^E \quad B_n{}^E=B_p{}^E+\lambda k_l/2M,$$
$$B^M=B_p{}^M+B_{n'}{}^M \quad B_n{}^M=B_p{}^M-(k_l/2M)(2\lambda+1),$$
$$A_p{}^E=-1+\Re(\mathrm{Re}\mathfrak{M})+\tfrac{1}{2}\mathrm{Re}\mathcal{E}+\tfrac{1}{2}i\mathrm{Im}\mathcal{E},$$
$$A_p{}^M=-k_l/2M+(1-\Re)\mathrm{Re}\mathfrak{M}+i\mathrm{Im}\mathfrak{M},$$
$$B_p{}^E=-\lambda k_l/2M+\tfrac{1}{2}\Re(\mathrm{Re}\mathfrak{M})-\tfrac{1}{2}\mathrm{Re}\mathcal{E}-\tfrac{1}{2}i\mathrm{Im}\mathcal{E},$$
$$B_p{}^M=k_l/2M(\lambda+1)^2+\tfrac{1}{2}(1-\Re)\mathrm{Re}\mathfrak{M}+\tfrac{1}{2}i\mathrm{Im}\mathfrak{M},$$

where $(d\sigma/d\Omega)^{\text{c.m.}}$ = differential cross section for the deuteron Compton effect in the c.m. system; θ = photon scattering angle in the c.m. system; e = proton charge; M = proton mass; k_d = incident photon energy in the deuteron-photon c.m. system; k_l = incident photon energy in the lab system; $S(q)$ = "sticking factor"; A^E = deuteron electric spin-independent amplitude (lab); A^M = deuteron magnetic spin-independent amplitude (lab); B^E = deuteron electric spin-dependent amplitude (lab); B^M = deuteron magnetic spin-dependent amplitude (lab); $A_{p,n}{}^{E,M}$ $B_{p,n}{}^{E,M}$ are proton or neutron amplitudes equivalent to the analogous ones above for the deuteron; $\lambda=1.79$ = anomalous magnetic moment for the proton; $\mathcal{E}$ and $\mathfrak{M}$ are electric and magnetic pionic contributions to the amplitudes, plotted in Capps' first article; and $\Re$ is a function of the amplitudes, plotted in Capps' second article. $\Re$ is a correction to the earlier work by means of an additional dispersion relation.

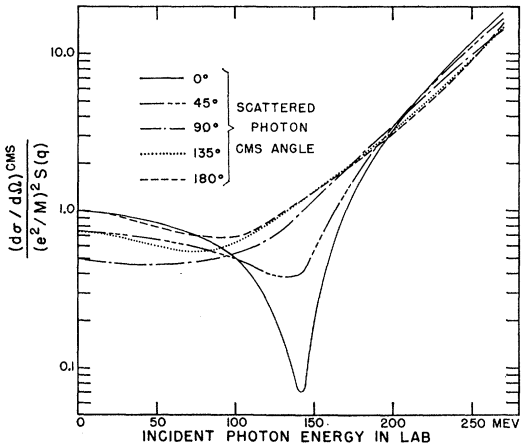

FIG. 11. The energy dependence of $d\sigma/d\Omega$ for various angles as given by calculations using the Capps' amplitudes.

The energy and angular dependence of the Capps' formula is shown by the series of curves in Figs. 11 and 12.

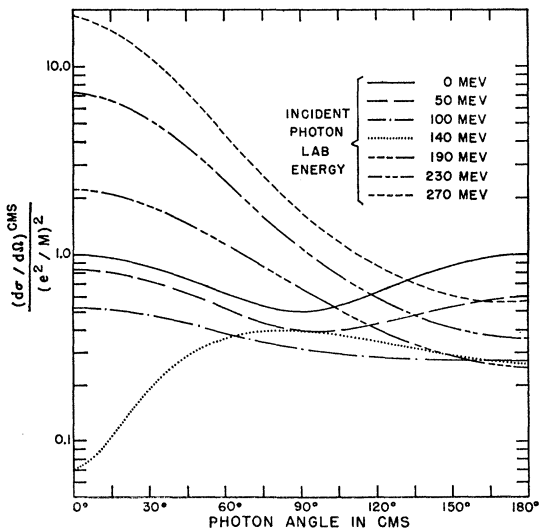

FIG. 12. The angular dependence of $d\sigma/d\Omega$ for various incident photon energies using Capps' amplitudes.

Jacob and Mathews Theory[6]

$$(d\sigma/d\Omega)^{\text{c.m.}}$$
$$= (e^2/M)^2[E_d/(E_d+k_d)]^2 S(q)[\tfrac{1}{2}|h_1|^2(1+y)^2$$
$$+\tfrac{1}{2}|h_2|^2(1-y^2)^2+(-\mathrm{Re}h_1^*h_2+\tfrac{2}{3}\mathrm{Re}h_3^*h_4$$
$$+4\mathrm{Re}h_5^*h_6-\tfrac{4}{3}\mathrm{Re}h_3^*h_5-\tfrac{4}{3}\mathrm{Re}h_4^*h_6)y(1-y^2)$$
$$-\tfrac{4}{3}\mathrm{Re}h_4^*h_5y^2(1-y^2)+\tfrac{2}{3}|h_5|^2(1-y^2)(1+2y^2)$$
$$+\tfrac{1}{3}|h_3|^2(3-y^2)+\tfrac{1}{3}|h_4|^2(1-y^4)$$
$$+(2|h_6|^2-(8/3)\mathrm{Re}h_3^*h_6)(1-y^2)],$$

$$y=\cos\theta,$$
$$h_i=f_{pi}+f_{ni}=2f_{pi}-\delta_i;$$
$$\delta_1=1,$$
$$\delta_2=-k_p,$$
$$\delta_3=k_p(1+2\lambda)(1-y),$$
$$\delta_4=\delta_5=-k_p(1+2\lambda),$$
$$\delta_6=k_p(1+\lambda)/2;$$

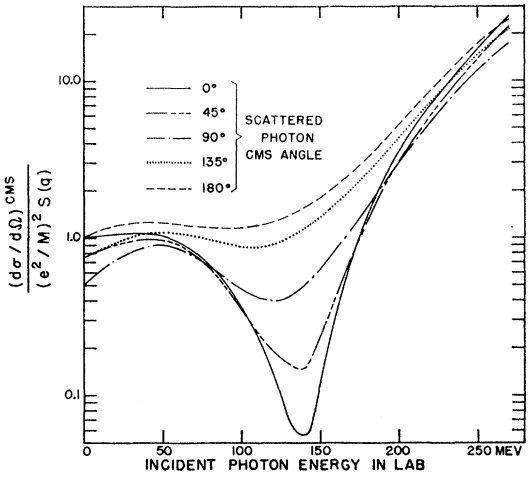

FIG. 13. The energy dependence of $d\sigma/d\Omega$ for various angles as given by calculations using the Jacob-Mathews amplitudes.

where $(d\sigma/d\Omega)^{\text{c.m.}}$ = differential cross section for deuteron Compton effect in the c.m. system; θ = photon scattering angle in the c.m. system; e = proton charge; M = proton mass; E_d = total deuteron energy in the c.m. system; k_d = incident photon energy in the deuteron-photon c.m. system; $S(q)$ = "sticking factor"; h_i are deuteron amplitudes in the lab system; f_{pi}, f_{ni} are proton and neutron amplitudes (lab); f_{pi} are tabulated in Jacob and Mathews' article; k_p = incident photon energy in the proton-photon c.m. system; $\lambda=1.79$ = anomalous magnetic moment of proton.

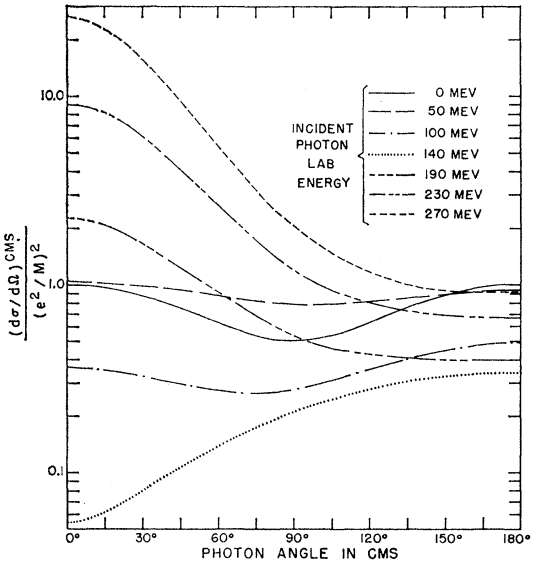

FIG. 14. The angular dependence of $d\sigma/d\Omega$ for various incident photon energies using Jacob-Mathews amplitudes.

The energy and angular dependence of the Jacob-Mathews curves is shown by the series of curves in Figs. 13 and 14.